

# Micro-plasticity of surface steps under adhesive contact: Part II – Multiple-dislocation mediated contact hardening

Y.F. Gao<sup>a,b</sup>, H.H. Yu<sup>c</sup>, K.-S. Kim<sup>d</sup>

<sup>a</sup> *Dept. of Materials Science and Engineering, University of Tennessee, Knoxville, TN 37996*

<sup>b</sup> *Computer Science and Mathematics Division, Oak Ridge National Lab, Oak Ridge, TN 37831*

<sup>c</sup> *Department of Mechanical Engineering, City College of New York, New York, NY 10031*

<sup>d</sup> *Division of Engineering, Brown University, Providence, RI 02912*

## Abstract

The study of the micro-plastic behavior of rough surface contact is the critical link towards a fundamental understanding of contact, friction, adhesion, and surface failures at small length scales. In the companion paper (Yu et al., *J. Mech. Phys. Solids* 55, 489-516, 2007), we have studied the onset of surface yielding due to single-dislocation nucleation from a stepped surface under adhesive contact. Here we analyze the contact hardening behavior due to multiple dislocations in a two-dimensional dislocation model. Continuum micromechanical analyses are used to derive the configurational force on the dislocation, while a modified Rice-Thomson model is used to describe the dislocation nucleation. Dislocations nucleated from a surface source are stabilized and pile up as a result of the balance between the resolved driving force and the non-zero lattice resistance in the solid. The dislocation pileup will exert a strong back stress to prevent further dislocation nucleation and thus lead to the contact hardening behavior, the degree of which depends on the slip-plane orientation. Particularly, we find that the dislocation interactions between two slip planes can make the contact loading order-of-magnitude easy to nucleate multiple dislocations, which is thus named “latent softening”. A mechanistic explanation shows that the latent softening is closely related to the mode mixity of the stress intensity at the surface step. Dislocation nucleation will modify the geometric characteristics of the surface step, so that the contact-induced stress state near the step, as described by the mode mixity, changes, which influences the subsequent dislocation nucleation. Our calculations show that the dislocation pileup on one slip plane can even cause spontaneous dislocation nucleation on the other slip plane without further increase of the contact load. Furthermore, it is found that the rough surface contact at small length scale can lead to the dislocation segregation and the formation of a surface tensile sub-layer. The discrete-dislocation model presented here provides novel insights in bridging the atomistic simulations and continuum plastic flow analysis of surface asperity contact. Implications of the theoretical predictions are also discussed.

*Keywords:* Contact mechanics; Surface micro-plasticity; Dislocation model; Surface step; Hardening anisotropy; Latent softening

## 1. Introduction

Surfaces of most engineering materials are unavoidably rough, and contain geometric irregularities with feature sizes ranging from nanometers to micrometers. Many important mechanical properties and failure problems, such as contact fatigue and friction, are not determined by macroscopic contact nor is it determined on the atomic level. Recent technological advancements (Forrest, 2004), such as nanostructure fabrication (e.g., nano-imprinting, cold-welding, chemical-mechanical planarization), require a fundamental understanding of rough surface contact, adhesion and friction at meso- and nano-scale. Despite the long-standing efforts on the study of rough surface contact, the role of surface micro-plasticity has not been sufficiently studied, particularly in the critical connection between microscopic and atomistic processes of deformation behavior and surface interactions (Gao and Bower, 2006; Pei et al., 2005; Zimmerman et al., 2001). One reason is the lack of the direct observation of near surface dislocation arrangements (Kim, 1980; Larson et al., 2002). Here the study of surface micro-plasticity considers the dislocation-based plastic deformation near and at the rough surface, i.e., dislocation nucleation and annihilation at the rough surface and the dislocation multiplication and interaction underneath. Though roughness root-mean-square amplitude may be confined to a very thin layer, the resulting dislocation pileup can extend to a far distance, and potentially interact with bulk plastic field.

A model of micro-plastic deformation of surface steps by the single-dislocation nucleation was studied under a multiscale framework in the companion paper (Yu et al., 2007). A dislocation can be nucleated from the stress concentration at the surface step under a combination of remote load and interface adhesion. The dislocation nucleation process is modeled by both the atomistic simulation and the continuum Rice-Thomson criterion (Rice and Thomson, 1973), while atomistic simulations can be used to calibrate the constitutive parameters used in the Rice-Thomson model. The configurational force on the dislocation can be computed by using the Stroh formalism (Stroh, 1958; Suo, 1990; Gao and Pharr, 2007) and the conservation integrals (Eshelby, 1970). Contact strength map of dislocation nucleation can be constructed with respect to varying parameters such as interface adhesion, step size and lattice resistance. The geometry of the surface steps and the slip systems of easy glide segregate two types of dislocations at equilibrium positions either close to or away from the interface. Nevertheless, the nucleation and stabilization of the first dislocation from a surface step is still

confined to a very small length scale. However, it is not clear how it is related to realistic applications since the dislocation pile-up process and the interaction between neighboring slip systems are responsible for the hardening behavior of surface micro-plasticity. This is analyzed in detail in this paper.

Figure 1 depicts the surface-step contact model with multiple dislocations. The stepped substrate is indented by a rigid platen from the above. The interface gap is treated as an interface crack with size  $a$ , which is determined by the Griffith condition (i.e., balancing the energy release rate and the work of adhesion at the right crack tip). Consequently, the crack size  $a$  is a function of the elastic constants of solid II  $c_{ijkl}$ , the applied load  $\mathbf{T}^\infty$ , the interface work of adhesion  $\Gamma_{adh}$ , the step size  $h$ , and the Burgers vectors and locations of dislocations. The solid II embeds a pile-up of  $N$  dislocations of locations  $(r_k, \theta_k)$  and Burgers vectors  $\mathbf{b}_k$ , where  $\theta = \tan^{-1}(x_2/x_1)$ . Perfect bonding is assumed outside the interface crack. We consider two types of slip planes:  $\theta = -3\pi/4$  and  $\theta = -\pi/4$ . Our micromechanical model treats those dislocations as elasticity singularities; the effect of core structure and short-range interaction are not considered. The dislocations, after nucleated and stabilized in the substrate, leave behind negative counterparts at the surface step and thus change the surface topography. The surface step is treated by inserting an extra layer of materials into  $x_1 < 0$ , and modeled by a super-dislocation with the Burgers vector  $\boldsymbol{\delta} = (0, h, 0)^T$  and step height  $h$ . After the emission of a number of dislocations, the surface step changes to  $\boldsymbol{\delta} - \sum_k \mathbf{b}_k$ . The companion paper (Yu et al., 2007) investigates the critical condition for the single dislocation nucleation from the surface step, while the present paper is interested in the plastic behavior of the stepped surface that is mediated by the pileup and interactions of multiple dislocations on multiple slip planes.

This paper is arranged as follows. Section 2 discusses the energetics calculation of the driving force on multiple dislocations and the dislocation nucleation criterion. Results of dislocation nucleation and pileup on single slip planes are presented in Section 3, and results for interactions of dislocations on two slip planes are given in Section 4. Section 4 also develops a mechanistic explanation of the novel cooperative hardening behavior based on the mode mixity at the stress concentration. Validity of assumptions in our micromechanical model and

implications on the experimental applications will be discussed in Section 5. Concluding remarks for this and the companion papers are given in Section 6.

## 2. Energetics and nucleation conditions for multiple dislocations

The driving force on a dislocation can be computed from the external stress field by the Peach-Koehler formula. To determine the stress fields, we use the anisotropic elasticity solution method developed by Stroh (1958) and the analytic continuation method for bi-material interface cracks by Suo (1990), as summarized in the appendices of the companion paper (Yu et al., 2007). The driving force can also be interpreted as the decrease of the total potential energy with respect to the dislocation location. Therefore, we can use the  $M$  and  $J$  conservation integrals (Eshelby, 1970) to obtain an elegant representation. The elastic fields caused by the dislocation pileup in Fig. 1 can be solved using the linear superposition scheme in Fig. 2. For the  $k$ -th dislocation, the driving force has two parts. The first one is the driving force when there is only the  $k$ -th dislocation itself, as in Fig. 2(a). The second part is the summation of interaction forces from all other dislocations, as in Figs. 2(b), 2(c), etc. Consequently, the driving force on the  $k$ -th dislocation is

$$J_k = -\frac{\partial \Pi}{\partial r_k} = J_k^{\text{single}} + \sum_{l \neq k} J_{lk}^{\text{int}}, \quad (1)$$

where  $\Pi$  is the elastic potential energy,  $J_k^{\text{single}}$  is the driving force due to the  $k$ -th dislocation only, and  $J_{lk}^{\text{int}}$  is the driving force on the  $k$ -th dislocation due to the  $l$ -th dislocation pair ( $l \neq k$ ). The representations of driving forces and the calculation procedure are specified in the Appendix A of this paper. In addition, using conservation integrals, one can establish a relation of the driving forces on all the dislocations. This conservation condition, Eq. (A5), has been repeatedly checked in each step of our calculation.

If the contact is loaded with a quasi-static monotonic force  $\mathbf{T}^\infty$ , dislocations will glide to some distance away from the interface and will always be in equilibrium with the Peierls force  $G_p$ . The equations of static equilibrium for each dislocation take the mathematical form

$$J_k(\mathbf{r}_1, \mathbf{r}_2, \dots, \mathbf{r}_N; \mathbf{T}^\infty / c_{11}, h/b, \Gamma_{adh} / c_{11}b) - G_p = 0, \quad (2)$$

with  $k = 1, 2, \dots, N$ . Burgers vectors are  $\mathbf{b}_k = b(-\cos \theta_k, -\sin \theta_k, 0)^T$ , for which the magnitude  $b$  is the same for all dislocations. This provides a set of  $N$  equations for  $N$  dislocation positions

$\mathbf{r}_k$ , with given  $\mathbf{T}^\infty/c_{11}$ ,  $h/b$  and  $\Gamma_{adh}/c_{11}b$ , where  $\mathbf{T}^\infty = (\sigma_{21}^\infty, \sigma_{22}^\infty, \sigma_{23}^\infty)^\top$ . It should be noted that the calculation of the crack size  $a/b$  is implicit in (2), because the crack size can be solely determined by the above parameters and therefore is not an independent parameter. The solid I is assumed to be rigid, and the elastic constants of the solid II (substrate) are taken to be those of gold, i.e.,  $c_{12}/c_{11} = 0.67$  and  $c_{44}/c_{11} = 0.36$ .

We are interested in determining the contact hardening behavior, i.e. the relation between the applied contact pressure and the plastic deformation. The latter can be approximately described by the number of nucleated dislocations. The formation of a pile-up of  $N$  dislocations requires that some dislocation nucleation criterion must have been satisfied  $N$  times. Now consider an existing pile-up of  $N$  dislocations in solid II, the nucleation condition for the  $(N+1)$ -th dislocation can be formulated by a simple modification of the Rice-Thomson criterion for the nucleation of a single dislocation. Namely, the criterion for the nucleation of the  $(N+1)$ -th dislocation is that the driving force on the  $(N+1)$ -th dislocation (when placed at  $r = \eta$ ) reaches the Peierls force with a given set of fixed  $N$  dislocations whose equilibrium positions are obtained by  $N$  equations in Eq. (2). Because the equilibrium positions of existing dislocations are usually far away from the surface step, i.e.  $r_{k,eq} \gg \eta$  ( $k = 1, 2, \dots, N$ ), the test dislocation at  $r = \eta$  does not affect the equilibrium positions of the existing  $N$  dislocations. In general, there are  $N$  force-balance equations and  $N$  variables  $r_k$  (the orientations of the Burgers vector,  $\theta_k$ , are given a priori or determined one-by-one as shown in Section 4), and we use the Newton-Raphson method to determine the equilibrium positions. Figure 3 gives a typical result of this root finding procedure, with  $h/b = 50$ ,  $G_p/c_{11}b = 0.001$ ,  $\Gamma_{adh}/c_{11}b = 0.02$  and  $\sigma_{22}^\infty/c_{11} = -0.0015$ . All the dislocations are on the slip plane  $\theta = -3\pi/4$ . These given parameters ensures the nucleation of four dislocations with equilibrium positions,  $r_{eq}/b = 4435, 3588, 2862, 2156$ , respectively, corresponding to the vertical dashed lines in Fig. 3. We allow the movement of a given dislocation with the rest three fixed, and then calculate the driving force against the radial distance. The equilibrium position is the cross section of the driving force and the Peierls force. A dislocation, when placed very close to its neighbors, will be subjected to strong

repulsive force away from the neighbors, as shown by the diverging trends of those solid curves in Fig. 3.

The root finding process is very slow because of the multi-dimensional functions in Eq. (2) and the shallow slope of the driving-force curves in Fig. 3. The use of the conjugate gradient method or the viscous drag method suffers the similar problem when there are a large number of dislocations. Nor is it appropriate to treat the dislocation pileup by a continuous function of dislocation distribution because the discrete model is required for the study of dislocation nucleation from the surface step. Practically, we find out that it is quite accurate and efficient to calculate the driving force by treating near interface dislocations as discrete single-dislocations and those faraway ones as super-dislocations. For most of our results presented in this paper, we use the scheme of individual single-dislocations when  $r_{eq} < 10a$ , plus several super-dislocations when  $10a < r_{eq} < 100a$ , plus a super-dislocation when  $r_{eq} > 100a$ . For a super-dislocation with  $nb$ , the lattice resistance becomes  $nG_p$ .

### 3. Contact hardening mediated by multiple-dislocations on a single slip plane

Here we are interested in the conditions for the nucleation of additional dislocations with existing dislocation pileup in the substrate. In this section, we restrict our attention to single slip planes. The cooperation of multiple slip planes will be studied in the next section. The calculation in Figure 4 is specified as follows. Suppose that we have  $N - 1$  dislocations in the substrate. With a given contact load  $\sigma_{22}^\infty$  (other components of the applied traction are zero), we first determine the  $N - 1$  equilibrium positions, and then compute the driving force on the fictitious,  $N$ -th dislocation that is placed at  $r = \eta$ . Thus we generate a curve of  $\sigma_{22}^\infty$  against  $J_N$ . The load that ensures  $J_N = G_p$  is the critical load to nucleate this dislocation,  $\sigma_{crit,N}^\infty$ . Figure 4(a) considers the dislocations at slip plane  $\theta = -3\pi/4$  (hereafter referred to as dislocations at left slip plane, or simply left dislocations), and presents five curves of  $\sigma_{22}^\infty \sim J_N$  with  $N$  from 1 to 5. Figure 4(b) is for  $\theta = -\pi/4$  (hereafter referred to as right dislocations). Both plots show hardening behavior, that is, the increase of  $|\sigma_{22}^\infty|$  is needed to nucleate subsequent dislocations. However, these two slip planes show different degrees of contact hardening. It is easier to nucleate the first right dislocation than the first left one. To nucleate additional dislocations along

the left slip plane requires moderate increase of the applied load, while dramatic increase of contact pressure is needed for the right slip plane.

Another important difference between the two slip planes is that the dislocation pileups also segregate into places either close to or far away from the surface step. For the calculations presented in Fig. 4, the equilibrium positions of the left dislocations are on the order of  $1000b$ , and those of the right dislocations are about  $100b$ . Thus dislocation pileup and segregation of dislocations can happen at the same time. However, if two or more slip planes operate, the interaction between dislocation pileups on different slip planes can change this scenario. This will be examined in the next section.

Based on the calculations presented in Fig. 4, we can vary the controlling parameters and then construct maps for the nucleation conditions of multiple dislocations. As shown in Fig. 5, the contact hardening behavior is different not only for the two slip planes, but also for different step heights. For the left slip plane in Fig. 5(a), the critical load (in terms of the absolute value) to nucleate the first dislocation increases as the step size increases. For high steps, only a small increase of compressive load is needed to nucleate subsequent dislocations, while shallow steps require a large increase of compression. The trend is more evident as more and more dislocations are piled up underneath. It is also clear that the lower the Peierls barrier, the easier to nucleate additional dislocations. For the right slip plane in Fig. 5(b), the dependence of the critical load for multiple dislocation nucleation on the step size is similar to that for the nucleation of the first dislocation. For both slip planes, it will be extremely difficult to generate many dislocations for shallow steps, because the dislocation pileup is very close to the source, and thus gives rise to a strong back stress to prevent the subsequent dislocation nucleation. In addition, the increase of the work of adhesion  $\Gamma_{adh}/c_1b$  will shift up these curves in Fig. 5, meaning that the larger the adhesion, the easier for dislocation nucleation. The decrease of the Rice-Thomson length  $\eta$  will make dislocation-nucleation more difficult to occur, because of the dominance of attractive force between the dislocation and the step at small  $r$ .

#### 4. Latent softening due to interactions of dislocations on multiple slip planes

This section presents the results of the contact hardening behavior when the two slip planes are both activated. The calculation procedure in Fig. 4 needs to be modified. With existing  $n$  left dislocations and  $m$  right dislocations (hereafter denoted as  $(n, m)$  or RmLn), we compute

the  $\sigma_{22}^\infty \sim J$  curve for the  $(m+n+1)$ -th dislocation when it is placed at  $r = \eta$  with  $\theta = -3\pi/4$  or  $\theta = -\pi/4$ . We increase the contact pressure monotonically in a quasi-static manner, so that we can determine which slip plane is favored for the next dislocation nucleation, and then update the dislocation pileup to either  $(n+1, m)$  or  $(n, m+1)$ . A typical result is presented in Fig. 6, with  $h/b = 50$ ,  $G_p/c_{11}b = 0.001$  and  $\Gamma_{adh}/c_{11}b = 0.02$ . Referring to the nucleation maps in Fig. 5, it is much easier to nucleate the first several dislocations on the right slip plane than that on the left one, but dislocation pileup on the right slip plane causes a strong hardening, so that the dislocation nucleation on the left slip plane will eventually follow. Fig. 6(a) compares the  $\sigma_{22}^\infty \sim J$  curves for the left test dislocation (denoted by R4L2+L1) and the right test dislocation (denoted by R4L2+R1), which shows that the next dislocation nucleation event occurs on the right slip plane since it requires lower compression. In Fig. 6(b), it is found that, starting from R5L2 configuration, no increase of the applied load is required to nucleate a dislocation on the left slip plane, which is thus called spontaneous dislocation nucleation. The dislocation nucleations happen somehow alternatively between the two slip planes, i.e. (0,1), (0,2), (0,3), (1,3), (1,4)\*, (2,4), (2,5), (3,5)\*, (4,5), (4,6)\*, (5,6), etc., where the occurrence of the spontaneous dislocation nucleation is marked with an asterisk.

Summarizing results in Figs. 4 and 6, we plot the magnitude of the applied contact pressure against the number of nucleated dislocations in Figure 7. For the two-dimensional contact problem, the indenter displacement depends on the remote boundary conditions, which will diverge as the calculation cell size approaches infinity (Gao et al., 2006). Therefore, the number of dislocations is used to describe the degree of plastic deformation. When only one slip plane is allowed, the onset of surface yielding and the degree of contact hardening depend on the slip-plane orientation. Nucleation of the first dislocation is easy to occur for the right slip plane, which, however, shows strong hardening behavior. For the left slip plane, it is difficult to yield but it shows less evident contact hardening. When both of the two slip planes operate, we get a significant drop of the hardening curve, as shown by the curve with cross markers. Each step of the stairway-like hardening curve in Fig. 7 corresponds to one or many times of spontaneous dislocation nucleation events. We describe this hardening behavior as *latent softening*, where the word *latent* denotes the interaction between different slip planes. We have determined the equilibrium positions of those dislocation pileups on the two slip planes, which also segregate

into different distance away from the interface. Therefore, the formation of dislocation double-layer is anticipated for multiple dislocations near the interface. In Figs. 7(b) and 7(c), we study the effect of  $h/b$  on the hardening curves. For shallow steps (e.g.  $h/b = 10$ ), it is easy to yield along the left slip plane, as also shown in Fig. 5. Both slip planes show a strong contact hardening behavior, which is more evident for the right slip plane. Latent softening curve is also order-of-magnitude lower than the two hardening curves with single slip-planes. For high steps (e.g.  $h/b = 200$ ), it is easy to yield along the right slip plane, but hardening curve also rises up rapidly. Latent softening is more evident for higher steps, suggesting that more dislocations can be piled up under a rougher surface.

The latent softening behavior might be due to the mutual attraction between nucleated dislocations at different slip planes. This is an appealing explanation, since the calculation shows alternating nucleation from the two slip planes. However, the existing dislocations are quite far away from the surface step, and the interaction between those dislocation pileups is not believed to be very large. Actually, there are two important factors for the latent softening behavior. First, the dislocation pileups generate back stress near the surface step, and change the characteristics of the stress intensity there. Second, when one dislocation is nucleated, a negative dislocation is left at the surface step; the Burgers vector of the surface step is modified by  $\delta - \sum_k \mathbf{b}_k$ .

According to the Rice-Thomson model, the dislocation nucleation is determined by the state of the resolved shear stress on the slip plane near the surface step. The elastic field can be characterized by the stress intensity factors and the mode mixity, as shown in the Appendix B. Figure 8 plots the evolution of the mode mixity angle at the surface step as a function of applied contact pressure (negative sign means compression), following the history of dislocation nucleation and pileup by the latent softening curve in Fig. 7(a). The sequence is given by A, B, C... The mode mixity at the right crack tip has negligible change, so that it is not considered here. As the alternating nucleation of dislocations on the two slip planes, the mode mixity angle oscillates, suggesting the back-and-forth change of positive and negative mode II components. With dislocations accumulated along one slip plane, the stress field will build up a mode II component that favors the nucleation of dislocation on the other slip plane. When dislocation pileup at one slip plane induces a significant change of mode mixity, a dislocation can be nucleated spontaneously (i.e. without increasing compression) on the other slip plane. For

example, the jump from point C to D and to E corresponds to the nucleation of a right dislocation followed by a spontaneous nucleation of a left dislocation.

## 5. Discussion

### 5.1. *Near Surface Dislocation Microstructure and Experimental Comparison*

This paper and the companion one (Yu et al., 2007) examine a unit-process model of the contact micro-plastic behavior of a stepped surface. The main results in the present paper show the transition from the yielding behavior controlled by single-dislocation nucleation to the hardening behavior governed by multiple dislocation interactions. As we have pointed in the companion paper (Yu et al., 2007), the present theoretical work is analogous to the studies of scale effects in friction of single-asperity contacts (Hurtado and Kim, 1999a, 1999b). In the companion paper, we suggest the formation of a dislocation double layer because of dislocation segregation. This paper re-examines this conclusion when there are multiple dislocations on multiple slip planes. Our results also confirm that dislocation pileups are segregated primarily due to the remote traction. Because of kinematic constraints, dislocations nucleated from the surface source have different characteristics at different slip planes, as shown by the Burgers vectors in Fig. 1. As a consequence, the resolved Peach-Koehler forces on different slip planes drive the dislocation pileups either towards the interface (thus described as anti-load dislocations) or away from the interface (thus described as pro-load dislocations). For surface steps with moderate height, the interaction between dislocations piled up at different slip planes is not strong enough to overcome this type of remote-traction-induced segregation. Consequently, the conclusion of dislocation segregation and the formation of dislocation double layer still hold for multiple-dislocation mediated surface plasticity, as shown by the schematic in Fig. 9(a). However, when there are a large number of dislocations or a large lattice resistance, the tail pro-load dislocations might be on the same depth as the leading anti-load dislocations. As a consequence, the segregation of dislocation pileups may not be very evident, and the lateral tensile stress might be quite weak.

The theoretical predictions are compared to two experiments. First, in Fig. 9(b), the plate impact experiment on a MgO single crystal (Kim, 1980) shows two types of dislocation slip lines emanating from the surface. Although we do not know the Burgers vectors, the formation of long and short slip lines qualitatively agrees with our prediction in Fig. 9(a). The bulk dislocation

sources are usually not activated. We believe that this is mainly because the strong lattice resistance of MgO crystal and the scarce density of bulk dislocation sources. For soft crystals, such as gold and aluminum, bulk dislocation sources can be easily activated, and will cause surface roughening, while the surface sources instigate surface smoothing, in the plastic deformation of the contacting surface. A bulk source can emit dislocations that might either prevent or facilitate the dislocation propagation from the surface source, leading to a rich diversity of micro-plastic behaviors. Second, the formation of the dislocation double layer in Fig. 9(a) will lead to a surface layer with tensile residual stress. Neither continuum Mises plasticity nor crystal plasticity will give rise to this phenomenon. This is confirmed by the experiments in Wang et al. (2006). They have developed a novel method to measure the curvature change during the progressive etching of contact loaded surface of a thin aluminum disk. The contact loading generated the residual stress prior to the etching. The depth profile of the residual stress can be deduced from the etching-induced curvature evolution from the Stoney equation (Freund and Suresh, 2004). The tensile residual stress layer is found to be about 300nm thick, and the magnitude is about 200MPa. Our prediction shows that the layer thickness depends on the surface roughness magnitude and wavelength. If the contact plasticity is dominated by bulk dislocation sources, the nucleated dislocations can directly annihilate at the surface, and dislocation segregation will not occur and there will be no tensile residual-stress layer.

## 5.2. *Validity of Assumptions in the Dislocation Model*

One question arises as to whether our theoretical predictions are sensitive to the assumptions in our micromechanical model. First, the latent softening behavior crucially depends on the dislocation nucleation criterion. The Rice-Thomson model is based on the stress state at the stress concentration, so that the mode mixity is responsible for the latent softening. Other types of dislocation nucleation criteria might substantially change this scenario. Second, the nucleated dislocation pileups are segregated mainly by the remote traction, and therefore the formation of dislocation double layer is independent of the dislocation nucleation criterion. Third, the dislocation nucleation criterion adopted in this work does not consider the three-dimensional nature of embryo dislocation (Rice and Beltz, 1992). To this end, the parameter  $\eta$  should be interpreted as a phenomenological parameter, and therefore needs to be determined by fitting to the atomistic simulation (Yu et al., 2007). A continuum cohesive zone model can also

be employed to capture more details of the dislocation nucleation process (Rice, 1992; Gao and Bower, 2004). Fourth, since the dislocation nucleation is significantly influenced by the mode mixity of the interface crack tip at the surface step, some of our conclusions might be changed if the interface is not perfectly bonded outside the crack. Any interface slip will have similar effects as applying shear traction on dislocation multiplication and pileup. It should be noted that the interface slip may also be governed by the nucleation and pileup of interface dislocations, as have been examined in Hurtado and Kim (1999a, 1999b). The competition and interaction of interface slip and subsurface dislocation activities will be an interesting topic for future research.

### 5.3. *Implications in the Rough Surface Contact*

The unit-process model of surface steps under adhesive contact can be used as a building block for a statistical model of rough surface contact. The interaction between neighboring steps will be a critical link. This is different from the classic statistical model that uses the continuum plastic flow theory and the distribution of contacting asperities (Gao and Bower, 2006), in which the plastic deformation is highly confined, and the lateral interaction between neighboring contacts is less important than the interaction at the normal direction. The lateral interaction based on the present surface-step contact model is radically different, as evidenced from the spreading slip lines in Fig. 9(b). We have also shown that dislocations nucleated from neighboring surface steps can form a Lomer junction, and thus prevent more dislocation nucleation (Yu et al., 2007). This phenomenon can be described as *neighboring hardening*. The neighboring steps can exert a lateral stress to a surface step and may significantly affect the mode mixity at the stress concentration. The lateral stress along  $x_1$  axis may be important when the dislocation nucleation criterion is affected by the coupling between normal and shear stresses (Rice and Beltz, 1994). Obviously, the lateral interaction between neighboring unit-processes depends on the spacing between them.

Using a two-dimensional discrete dislocation dynamics model, Nicola et al. (2007) investigated the competition between the surface-source-governed and bulk-source-governed behavior. It should be noted that they use a flat ended punch to mimic the stepped surface, and employ Frank-Read-type sources on the surface. This is different from our surface sources at surface steps. For their implementation, the mode mixity evolution might not play a significant role on the contact hardening behavior, but the segregation of dislocations nucleated from

surface sources still appears since this is primarily driven by the applied contact stress field. Their results also suggest that when both surface and bulk sources are present, the response is generally dominated by the bulk sources, so that the latent softening behavior and the tensile residual-stress layer will not be observed. This agrees with our discussion in Fig. 9(b), since the bulk sources in MgO are not actually activated and the dislocation slip lines are generated from surface sources.

Several implications in applications can be easily obtained from our theoretical analyses. For example, even if the adhesion energy can be very small between two smooth surfaces, adhesion can nevertheless lead to the dislocation-mediated surface micro-plastic deformation for a rough surface contact, thus giving rise to a severe stiction problem. Clearly, using classic continuum plasticity has little relevance to this problem. For shallow steps, a few dislocations can dramatically change the stress field near the surface step, so that the hardening behavior is more evident. Therefore it will be difficult to fully squash a shallow step. To achieve a large contact conformity, we need to promote the occurrence of the latent softening behavior, because the dislocation population and density can be dramatically increased under a given contact load.

## **6. Summary**

In this paper and the companion one, we have conducted a micromechanical dislocation analysis of the stepped surface contact, and examined the surface micro-plastic behavior due to the dislocation nucleation and pileup. The companion paper has constructed contact strength maps of the single dislocation nucleation by using the formulation of configurational force on the dislocation and the Rice-Thomson dislocation nucleation criterion. The Rice-Thomson model has also been calibrated by comparing the continuum dislocation model to the atomistic simulations. We have found that the surface step can emit dislocations along different slip planes, which are segregated into different distances from the interface mainly by the remote traction. Consequently, those pro-load and anti-load dislocations form the dislocation double layer. The present paper studies the multiple dislocation nucleations and the contact hardening behavior. Multiple dislocations can be nucleated and pile up near the rough surface, and usually form distinctive slip lines (in two dimensional view). We still treat the dislocations in discrete manner and compute the configurational forces by using the Stroh formalism and the conservation integrals. We have found that nucleated dislocations generate back stress at the

surface dislocation source, leading to contact hardening behavior, the degree of which depends on the slip-plane orientation (thus called anisotropic hardening). The cooperative hardening between different slip planes can be order-of-magnitude weaker than the single-slip-plane hardening curve. This type of *latent softening* behavior is related to the mode mixity at the stress concentration of the surface dislocation source. Multiple dislocation pileups and latent softening behavior can still show the formation of the dislocation double layer, because those dislocations are segregated mainly due to the remote tractions. The theoretical work reported here can help us establish a statistical model of rough surface contact based on the interaction between neighboring surface steps and between surface and bulk dislocation sources. Consequently, we will be able to construct a scale-bridging model for the study of the small-scale contact conformity and interaction between adhesion and dislocation-based surface plasticity.

### Acknowledgements

This work was supported by the General Motors/Brown Collaborative Research Laboratory at Brown University and by the Materials Research Science and Engineering Center at Brown University (NSF Grant DMR-0520651). Research at the Oak Ridge National Laboratory was sponsored by the Division of Materials Science and Engineering, Office of Basic Energy Sciences, U.S. Department of Energy, under contract DE-AC05-00OR22725 with UT-Battelle, LLC. The authors are grateful to helpful discussions with Y.T. Cheng, A.F. Bower, L. Nicola, and A. Needleman.

### Appendix A: Dislocation interaction and driving force

We first consider only one single dislocation inside the solid II, as shown in Fig. 2(a). The dislocation is placed at  $(r_k, \theta_k)$  (or in vector form  $\mathbf{r}_k$ ), and has the Burgers vector  $\mathbf{b}_k$ . The surface step is thus characterized by a super-dislocation with Burgers vector  $\boldsymbol{\delta} - \mathbf{b}_k$ . Subscript  $k$  denotes the  $k$ -th dislocation. The driving force on one single dislocation has been given in the companion paper (Yu et al., 2007). For clarity and convenience, we re-write the driving force as:

$$J_k^{\text{single}} = \frac{1}{r} \left[ \frac{1}{2\pi} \boldsymbol{\delta}^T \mathbf{H}^{-1} \boldsymbol{\delta} - \frac{1}{2\pi} \mathbf{b}_k^T (\mathbf{B}_{\text{II}} + \overline{\mathbf{B}}_{\text{II}})^{-1} \mathbf{b}_k + M_k^* \right] + J_k^\infty, \quad (\text{A1})$$

with

$$J_k^\infty = \left[ \left( \boldsymbol{\sigma}_\Pi^\infty \cdot \mathbf{b}_k \right) \times (0, 0, 1)^T \right] \cdot (\mathbf{r}_k / |\mathbf{r}_k|), \quad (\text{A2})$$

$$M_k^* = \frac{\bar{\mathbf{w}}^T (\mathbf{H} + \bar{\mathbf{H}}) \mathbf{w}}{4 \cosh^2 \pi \varepsilon} \left( \tilde{K}_{a,k} \bar{K}_{c,k} a^{-\frac{1}{2}-i\varepsilon} + \bar{\tilde{K}}_{a,k} K_{c,k} a^{-\frac{1}{2}+i\varepsilon} - \left| K_{(a+b),k} a^{\frac{1}{2}+i\varepsilon} \right|^2 \right) \\ + \frac{1}{8} \mathbf{w}_3^T (\mathbf{H} + \bar{\mathbf{H}}) \mathbf{w}_3 \left( 2 \tilde{K}_{3a,k} K_{3c,k} a^{-\frac{1}{2}} - \left| K_{3(a+b),k} a^{\frac{1}{2}} \right|^2 \right). \quad (\text{A3})$$

Eq. (A2) is the driving force on the dislocation from the remote traction when the dislocation is placed into a perfectly bonded bi-material without any surface step. The stress field  $\boldsymbol{\sigma}_\Pi^\infty$  is thus uniform, and can be easily determined from the remote traction  $\mathbf{T}^\infty$  and boundary conditions. In Eq. (A3), matrices  $\mathbf{H}$  and  $\mathbf{B}_\Pi$ , vectors  $\mathbf{w}$  and  $\mathbf{w}_3$ , and scalar  $\varepsilon$  are solely determined by the elastic constants of the two solids, and  $\tilde{K}_{a,k}$ ,  $\tilde{K}_{3a,k}$ ,  $K_{c,k}$ ,  $K_{3c,k}$ ,  $K_{(a+b),k} = K_{a,k} + K_{b,k}$  and  $K_{3(a+b),k} = K_{3a,k} + K_{3b,k}$  are given by Eqs. (E8), (D3), (B6) and (C4) in Part I, with the substitution of  $r_k$ ,  $\theta_k$  and  $\mathbf{b}_k$  for  $r$ ,  $\theta$  and  $\mathbf{b}$ . The subscripts  $a, b, c$  correspond to the three sub-problems in Fig. 3 in Yu et al. (2007).

Next, we consider a pileup of dislocations as shown in Fig. 1. The elastic fields can be determined by using the linear superposition scheme in Fig. 2. The driving force on the  $k$ -th dislocation is given in Eq. (1), where  $J_k^{\text{single}}$  is given in Eq. (A1), and  $J_{lk}^{\text{int}}$  is the driving force on the  $k$ -th dislocation due to the  $l$ -th dislocation pair ( $l \neq k$ ). This interaction force  $J_{lk}^{\text{int}}$  can be determined by the Peach-Koehler formula, namely,

$$J_{lk}^{\text{int}} = \left[ \left( \boldsymbol{\sigma}_\Pi^l(\mathbf{r}_k; \mathbf{r}_l, \mathbf{b}_l) \cdot \mathbf{b}_k \right) \times (0, 0, 1)^T \right] \cdot (\mathbf{r}_k / |\mathbf{r}_k|), \quad (\text{A4})$$

where  $\boldsymbol{\sigma}_\Pi^l(\mathbf{r}_k; \mathbf{r}_l, \mathbf{b}_l)$  is the stress field at  $\mathbf{r}_k$  due to a dislocation dipole of Burgers vector  $\mathbf{b}_l$  at  $\mathbf{r}_l$  and  $-\mathbf{b}_l$  at the coordinate origin. The boundary value problem specified in Figs. 2(b) and 2(c) can be easily determined from the bi-material fracture mechanics. The Stroh formulism for the bi-material problem will give all the stress components from one complex function vector  $\mathbf{h}(z)$  (Suo, 1990; Yu et al., 2007). The interaction between a dislocation-dipole and a bi-material interface crack can be decomposed into two problems. One involves placing a dislocation at the left crack tip, in which  $\mathbf{h}(z)$  is given by Eq. (C2) in Part I with  $\mathbf{d} = -\mathbf{b}_l$ . The other problem involves placing a dislocation at  $\mathbf{r}_l$ , in which  $\mathbf{h}(z)$  is a combination of Eq. (B4) in Part I and

$\mathbf{H}^{-1}\bar{\mathbf{H}}\mathbf{L}_{\text{II}}\mathbf{f}'_{\text{II}}(z)$  with  $\mathbf{f}_{\text{II}}(z)$  given by Eq. (B1b) in Part I. Once the stress field is obtained, we can compute the interaction force  $J_{lk}^{\text{int}}$  by using Eq. (A4) in this paper.

Using  $M$  and  $J$  conservation integrals, we can write down the following equation for the driving forces:

$$\sum_k (J_k - J_k^\infty) r_k = \frac{1}{2\pi} \boldsymbol{\delta}^T \mathbf{H}^{-1} \boldsymbol{\delta} - \frac{1}{2\pi} \sum_k \mathbf{b}_k^T (\mathbf{B}_{\text{II}} + \bar{\mathbf{B}}_{\text{II}})^{-1} \mathbf{b}_k + M^{**}, \quad (\text{A5})$$

where

$$M^{**} = \frac{\bar{\mathbf{w}}^T (\mathbf{H} + \bar{\mathbf{H}}) \mathbf{w}}{4 \cosh^2 \pi \varepsilon} \left( \tilde{K}_a \bar{K}_c a^{-\frac{1}{2}-i\varepsilon} + \bar{\tilde{K}}_a K_c a^{-\frac{1}{2}+i\varepsilon} - \left| K_{(a+b)} a^{\frac{1}{2}+i\varepsilon} \right|^2 \right) + \frac{1}{8} \mathbf{w}_3^T (\mathbf{H} + \bar{\mathbf{H}}) \mathbf{w}_3 \left( 2\tilde{K}_{3a} K_{3c} a^{-\frac{1}{2}} - \left| K_{3(a+b)} a^{\frac{1}{2}} \right|^2 \right), \quad (\text{A6})$$

with  $\tilde{K}_a = \sum_k \tilde{K}_{a,k}$ ,  $\tilde{K}_{3a} = \sum_k \tilde{K}_{3a,k}$ ,  $K_c = \sum_k K_{c,k}$ ,  $K_{3c} = \sum_k K_{3c,k}$ ,  $K_{(a+b)} = \sum_k K_{(a+b),k}$  and  $K_{3(a+b)} = \sum_k K_{3(a+b),k}$ . Eq. (A5) is used to test the calculation results of the driving forces from the superposition scheme in Fig. 2.

## Appendix B: Mode mixity at the step

If a crack can be characterized by three real stress intensity factors,  $K_{\text{I}}$ ,  $K_{\text{II}}$  and  $K_{\text{III}}$ , the mode mixity angle can be defined in the conventional way, i.e.  $\psi = \tan^{-1}(K_{\text{II}}/K_{\text{I}})$ . For our problem,  $K_{\text{III}}$  is always zero, and thus will not be discussed. If the stress intensity factors include a complex one  $K$  and a real one  $K_3$ , we have to introduce a length to define the mode mixity. Choosing different lengths only shifts the mode mixity angle. Using the step height gives

$$\psi = \tan^{-1} \left( \frac{\text{Im}(Kh^{-i\varepsilon})}{\text{Re}(Kh^{-i\varepsilon})} \right), \quad (\text{B1})$$

where  $\varepsilon$  is the oscillatory index of a bi-material interface crack. When  $\varepsilon = 0$ , Eq. (B1) degenerates into the conventional definition.

Since the dislocations are directly emitted from the left crack tip, i.e. the surface step, we need to calculate the mode mixity at  $(x_1 = 0, x_2 = 0)$ . The traction in the bonded interface at a distance  $r = -x_1$  ahead of the left crack tip is given by the asymptotic form:

$$\mathbf{t}(r) = \frac{1}{\sqrt{2\pi r}} \left( \bar{K}^L r^{-i\varepsilon} \mathbf{w} + K^L r^{i\varepsilon} \bar{\mathbf{w}} + K_3^L \mathbf{w}_3 \right), \quad (\text{B2})$$

so that the stress intensity factors can be easily extracted, namely,

$$\begin{aligned} \bar{K}^L &= \bar{K}_a^L + \bar{K}_b^L + \bar{K}_c^L = \sqrt{2\pi} \left( 1 + e^{-2\pi\varepsilon} \right) \lim_{x \rightarrow 0^-} (-x)^{1/2+i\varepsilon} h_1(x), \\ K_3^L &= K_{3a}^L + K_{3b}^L + K_{3c}^L = 2\sqrt{2\pi} \lim_{x \rightarrow 0^-} (-x)^{1/2} h_3(x), \end{aligned} \quad (\text{B3})$$

where

$$\begin{aligned} \bar{K}_a^L &= -\sqrt{2\pi} a^{-\frac{1}{2}+i\varepsilon} \frac{\bar{\mathbf{w}}^T \mathbf{H}}{\bar{\mathbf{w}}^T \mathbf{H} \mathbf{w}} \left( \mathbf{D} \left\{ q_j \left[ 1 - \left( \frac{s_j}{s_j - a} \right)^{-\frac{1}{2}+i\varepsilon} \right] \right\} + \bar{\mathbf{D}} \left\{ \bar{q}_j \left[ 1 - \left( \frac{\bar{s}_j}{\bar{s}_j - a} \right)^{-\frac{1}{2}+i\varepsilon} \right] \right\} \right), \\ K_{3a}^L &= -\sqrt{2\pi} a^{-\frac{1}{2}} \frac{\mathbf{w}_3^T \mathbf{H}}{\mathbf{w}_3^T \mathbf{H} \mathbf{w}_3} \left( \mathbf{D} \left\{ q_j \left[ 1 - \left( \frac{s_j}{s_j - a} \right)^{\frac{1}{2}} \right] \right\} + \bar{\mathbf{D}} \left\{ \bar{q}_j \left[ 1 - \left( \frac{\bar{s}_j}{\bar{s}_j - a} \right)^{\frac{1}{2}} \right] \right\} \right), \\ \bar{K}_b^L &= -\frac{1 + e^{-2\pi\varepsilon}}{\sqrt{2\pi}} a^{-1/2+i\varepsilon} \frac{\bar{\mathbf{w}}^T \mathbf{d}}{\bar{\mathbf{w}}^T \mathbf{H} \mathbf{w}}, \\ K_{3b}^L &= -\sqrt{\frac{2}{\pi}} a^{-1/2} \frac{\mathbf{w}_3^T \mathbf{d}}{\mathbf{w}_3^T \mathbf{H} \mathbf{w}_3}, \\ \bar{K}_c^L &= \sqrt{2\pi} \left( \frac{1}{2} - \varepsilon i \right) a^{1/2+i\varepsilon} \frac{\bar{\mathbf{w}}^T \mathbf{H} \mathbf{T}^\infty}{\bar{\mathbf{w}}^T \mathbf{H} \mathbf{w}}, \\ K_{3c}^L &= \sqrt{\frac{\pi a}{2}} \frac{\bar{\mathbf{w}}_3^T \mathbf{H} \mathbf{T}^\infty}{\bar{\mathbf{w}}_3^T \mathbf{H} \mathbf{w}_3}, \end{aligned} \quad (\text{B4})$$

and  $\mathbf{D}$ ,  $\mathbf{q}$ , and  $\mathbf{s}$  are given in Appendix B of Yu et al. (2007).

## References

- Eshelby, J.D., 1970. Energy relations and the energy-momentum tensor in continuum mechanics. In: Inelastic behavior of solids (ed. M.F. Kanninen, W.F. Adler, A.R. Rosenfield & R.I. Jaffee), pp. 77-115. New York: McGraw-Hill.
- Forrest, S.R., 2004. The path to ubiquitous and low-cost organic electronic appliances on plastic. *Nature* 428, 911-918.
- Gao, Y.F., Bower, A.F., 2004. A simple technique for avoiding convergence problems in finite element simulations of crack nucleation and growth on cohesive interfaces. *Modelling Simul. Mater. Sci. Eng.* 12, 453-463.
- Gao, Y.F., Bower, A.F., 2006. Elastic-plastic contact of a rough surface with Weierstrass profile. *Proc. R. Soc. A* 462, 319-348.
- Gao, Y.F., Bower, A.F., Kim, K.-S., Lev, L.C., Cheng, Y.T., 2006. The behavior of an elastic-perfectly plastic sinusoidal surface under contact loading. *Wear* 261, 145-154.
- Gao, Y.F., Pharr, G.M., 2007. Multidimensional contact moduli of elastically anisotropic solids. *Scripta Mater.* 57, 13-16.
- Hurtado, J.A., Kim, K.-S., 1999. Scale effects in friction of single-asperity contacts. I. From concurrent slip to single-dislocation-assisted slip. *Proc. Roy. Soc. London A* 455, 3363-3384.
- Hurtado, J.A., Kim, K.-S., 1999. Scale effects in friction of single-asperity contacts. II. Multiple-dislocation-cooperated slip. *Proc. Roy. Soc. London A* 455, 3385-3400.
- Kim, K.-S., 1980. Ph.D. thesis. Brown University. Providence, Rhode Island.
- Larson, B.C., Yang, W., Ice, G.E., Budai, J.D., Tischler, J.Z., 2002. Three-dimensional x-ray structural microscopy with submicrometer resolution. *Nature* 415, 887-890.
- Nicola, L., Bower, A.F., Kim, K.-S., Needleman, A., van der Giessen, E., 2007. Surface versus bulk nucleation of dislocations during contact. *J. Mech. Phys. Solids* *in press*. (doi:10.1016/j.jmps.2006.12.005)
- Pei, L., Hyun, S., Molinari, J.F., Robbins, M.O., 2005. Finite element modeling of elasto-plastic contact between rough surfaces. *J. Mech. Phys. Solids* 53, 2385-2409.
- Rice, J.R., Beltz, G.E., 1994. The activation-energy for dislocation nucleation at a crack. *J. Mech. Phys. Solids* 42, 333-360.
- Rice, J.R., Thomson, R., 1973. Ductile versus brittle behavior of crystals. *Phil. Mag.* 29, 73-97.

- Stroh, A.N., 1958. Dislocations and cracks in anisotropic elasticity. *Philos. Mag.* 3, 625-646.
- Suo, Z., 1990. Singularities, interfaces and cracks in dissimilar anisotropic media. *Proc. Roy. Soc. London A* 427, 331-358.
- Wang, J., Shrotriya, P., Yu, H.H., Kim, K.-S., 2004. Experimental measurements of surface residual stress caused by nano-scale contact of rough surfaces. *Mater. Res. Soc. Symp. Proc.* Vol. 795, U9.9.
- Yu, H.H., Shrotriya, P., Gao, Y.F., Kim, K.-S., 2007. Micro-plasticity of surface steps under adhesive contact. Part I. Surface yielding controlled by single-dislocation nucleation. *J. Mech. Phys. Solids* 55, 489-516.
- Zimmerman, J.A., Kelchner, C.L., Klein, P.A., Hamilton, J.C., Foiles, S.M., 2001. Surface step effects on nanoindentation. *Phys. Rev. Lett.* 87, 165507.

## Figure captions

- Figure 1 Schematic representation of a stepped solid indented by a rigid platen. With the nucleation of many dislocations, the resulting Burgers vector of the modified surface step is given by  $\delta - \sum_k \mathbf{b}_k$ , where  $\delta = [0, h, 0]^T$  and  $h$  is the original step height.
- Figure 2 The boundary value problem in Fig. 1 can be solved by the linear superposition scheme. The sub-problem in (a) has been solved in the companion paper (Part I). We also need to solve the sub-problems in (b), (c), etc., which involve dislocation dipoles, and then compute the interaction force on the dislocation  $\mathbf{b}_k$ .
- Figure 3 Equilibrium positions of the existing dislocations are determined by the Newton-Raphson root finding method. At the equilibrium positions, the driving forces (shown by the thick solid curves) are equal to the Peierls force for each of the four dislocations in this example. Other parameters are  $\theta = -3\pi/4$ ,  
 $\sigma_{22}^\infty/c_{11} = -0.0015$ ,  $h/b = 50$ ,  $\Gamma_{adh}/c_{11}b = 0.02$  and  $G_p/c_{11}b = 0.001$ .
- Figure 4 The driving forces are plotted in the two figures with varying applied load. The solid curves with markers, from top to bottom, correspond to the 1<sup>st</sup>, 2<sup>nd</sup>, and subsequent dislocations. The thin, solid vertical line denotes the Peierls force  $G_p/c_{11}b = 0.001$ . The cross sections of this line and the thick solid curves give rise to the critical load for dislocation nucleation. (a)  $\theta = -3\pi/4$ , and (b)  $\theta = -\pi/4$ . Other parameters are  $\Gamma_{adh}/c_{11}b = 0.02$ ,  $\eta/b = 5$  and  $h/b = 50$ .
- Figure 5 Critical loads for dislocation nucleation along a given slip plane are plotted against the step height. For  $\theta = -3\pi/4$  in (a), it is difficult to nucleate the first dislocation for large steps and the subsequent dislocations for small steps. Two sets of results are included for Peierls force  $G_p/c_{11}b = 0.001$  and  $G_p/c_{11}b = 0.0005$ . For  $\theta = -\pi/4$  in (b), the subsequent dislocation nucleations are very difficult for shallow steps. Parameters not shown are  $\eta/b = 5$  and  $\Gamma_{adh}/c_{11}b = 0.02$ . For (b),  $G_p/c_{11}b = 0.001$ .

- Figure 6 Procedure to determine the history of dislocation nucleation and pileup when two slip planes operate. (a) With existing R4L2 dislocations (4 dislocations on the right slip plane and 2 dislocations on the left slip plane), we plot the driving force on the 7<sup>th</sup> dislocation. For quasi-static loading, dislocation on the right slip plane ( $\theta = -\pi/4$ ) will be nucleated. (b) With existing R5L2 dislocations, it is found that no further compression is needed to nucleate the 8<sup>th</sup> dislocation on the left slip plane ( $\theta = -3\pi/4$ ), i.e., spontaneous dislocation nucleation. Additional parameters are  $\Gamma_{adh}/c_{11}b = 0.02$ ,  $\eta/b = 5$ ,  $h/b = 50$  and  $G_p/c_{11}b = 0.001$ .
- Figure 7 When a stepped surface is indented with increasing compressive load, dislocation activities along single slip planes and those with the cooperation of the two slip planes are radically different. (a)  $h/b = 50$ , (b)  $h/b = 10$ , and (c)  $h/b = 200$ . Additional parameters are  $\Gamma_{adh}/c_{11}b = 0.02$ ,  $\eta/b = 5$ , and  $G_p/c_{11}b = 0.001$ .
- Figure 8 Mode mixity angle,  $\psi = \tan^{-1}(\text{Im}(Kh^{i\varepsilon})/\text{Re}(Kh^{i\varepsilon}))$ , evolves with the history of dislocation nucleation and pileup, as indicated by the dashed curves (following A, B, C...). This plot corresponds to the latent softening curve (marked with crosses) in Fig. 7(a).
- Figure 9 (a) Schematic illustration of the segregation of dislocation pileups. (b) It is anticipated that the dislocation slip lines observed in the MgO impact experiment consist of different types of dislocation pileups. Those slip lines are made possible by the etch pit technique.

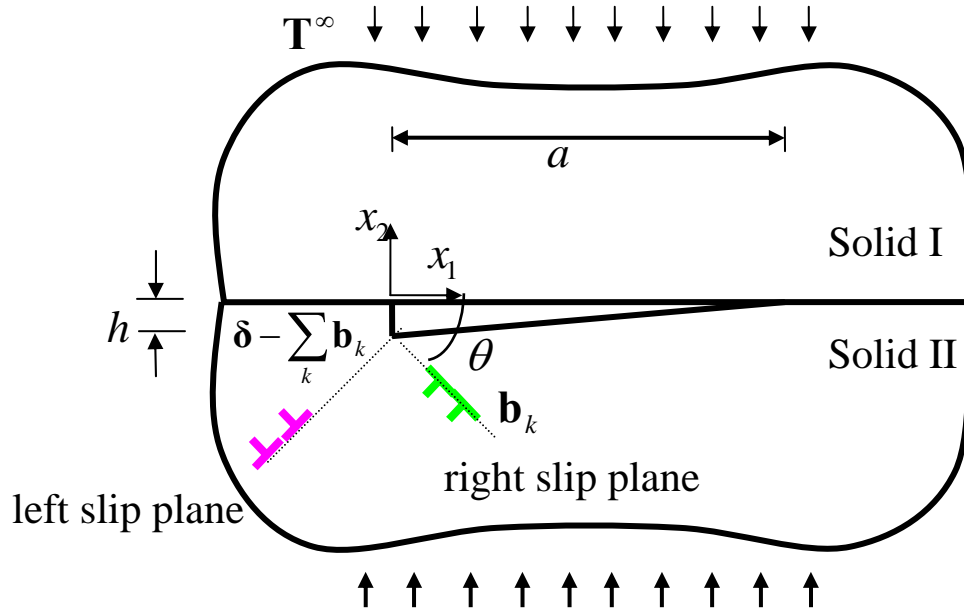


Figure 1

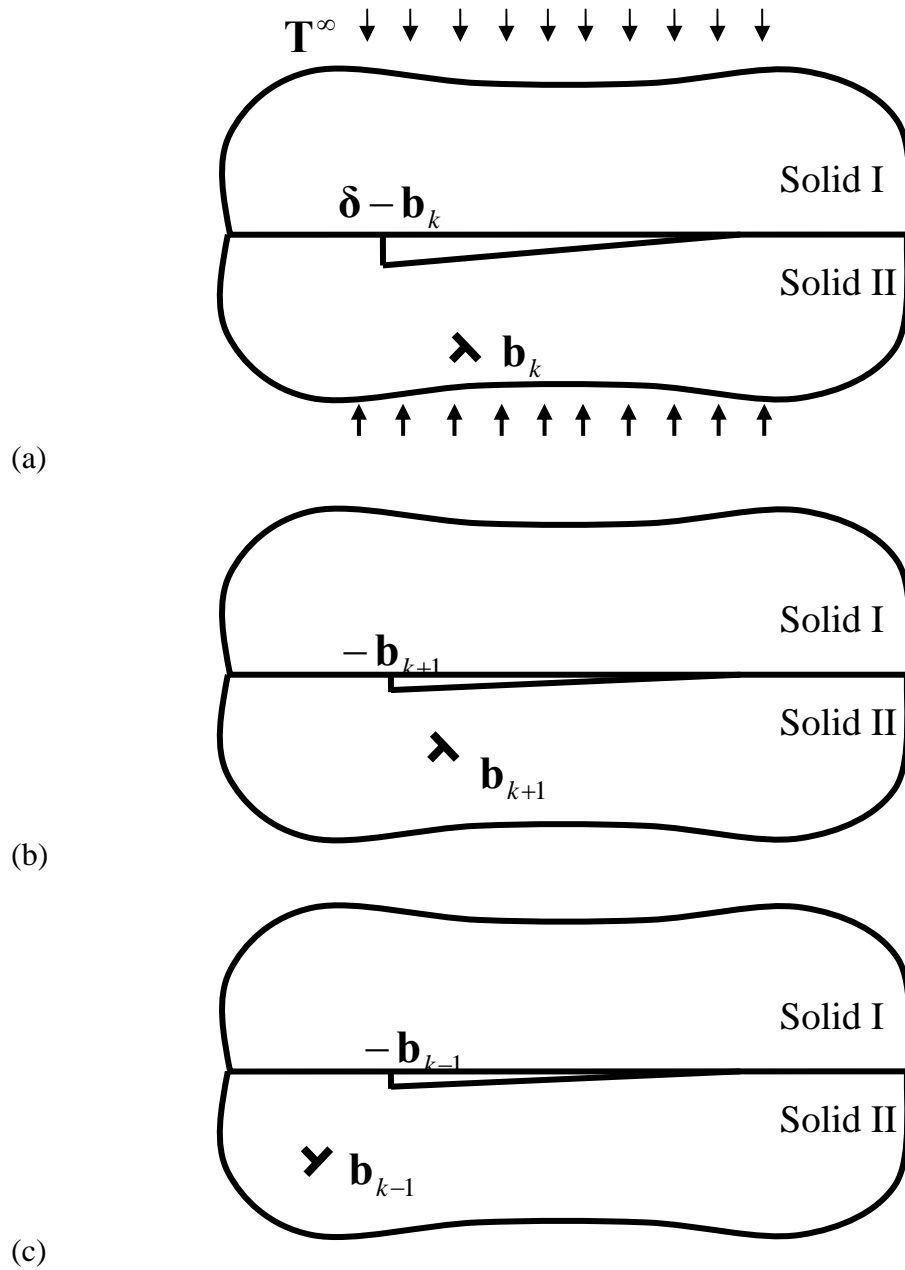


Figure 2

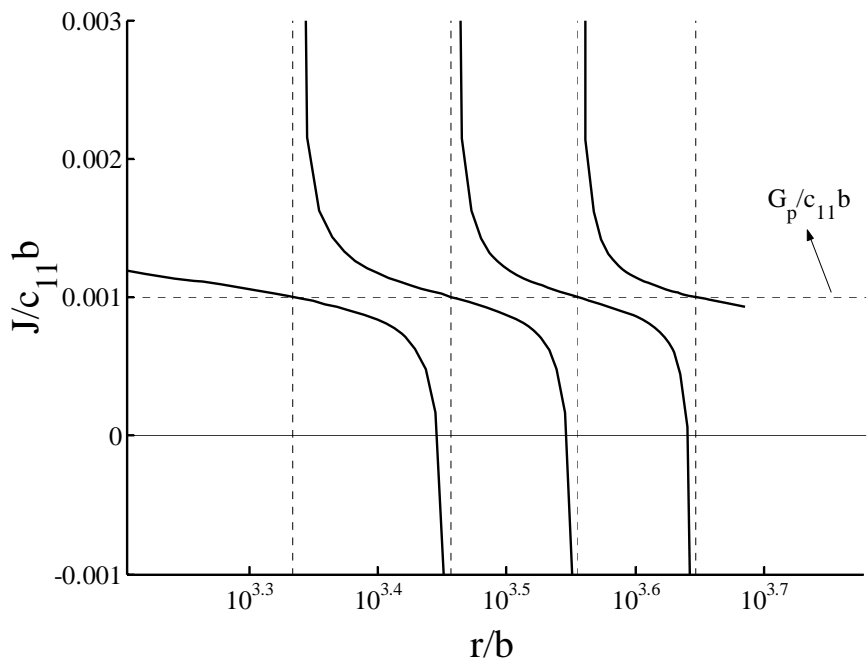
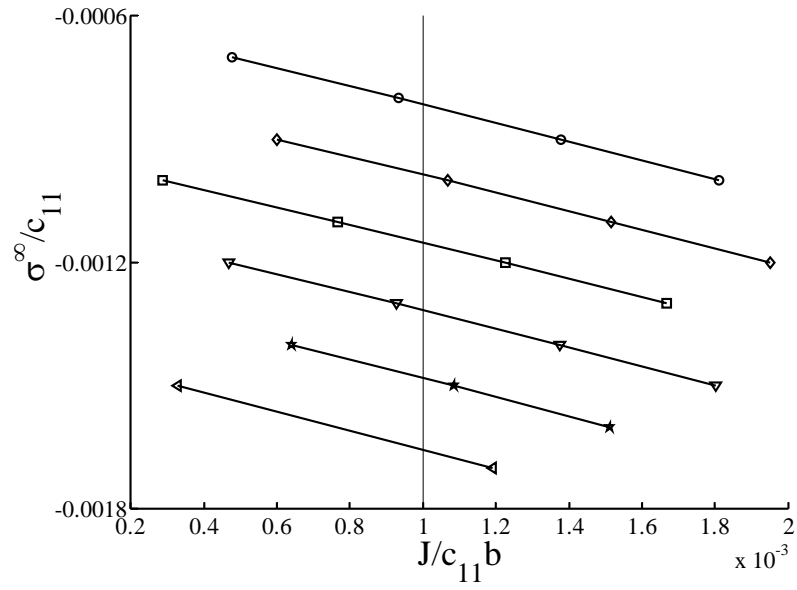
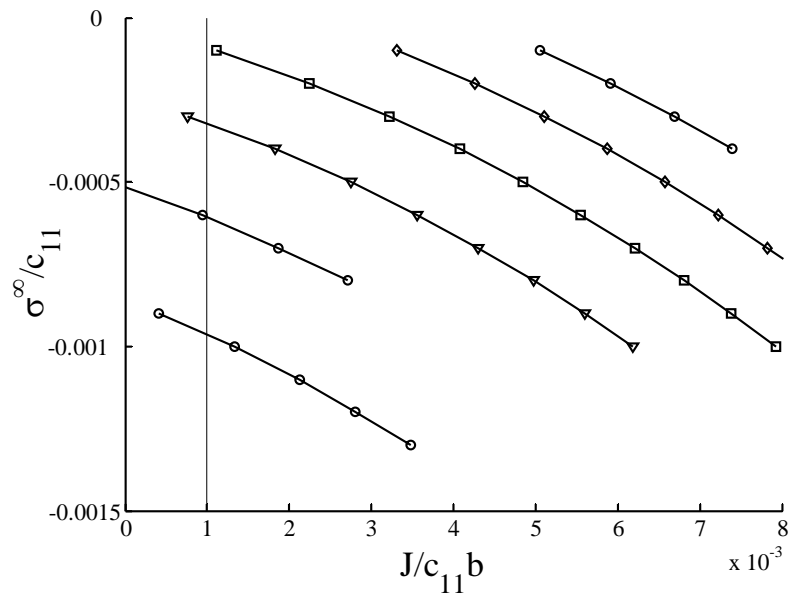


Figure 3

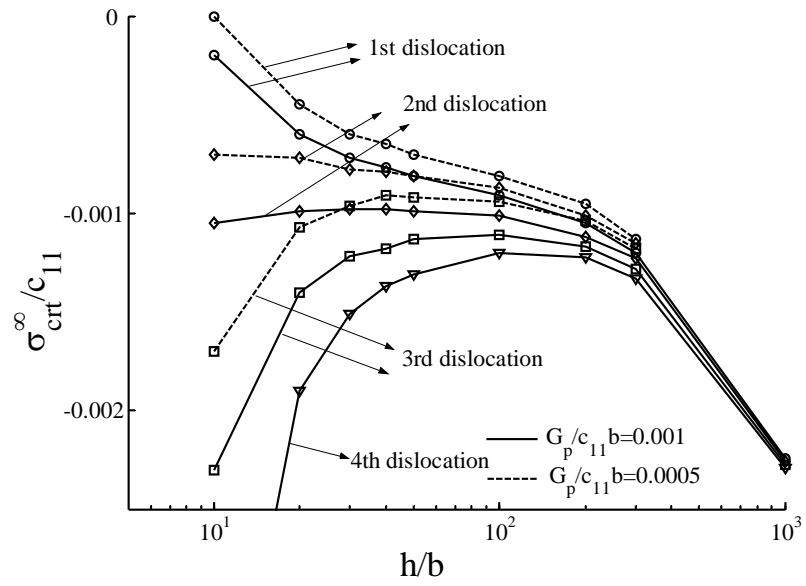


(a)

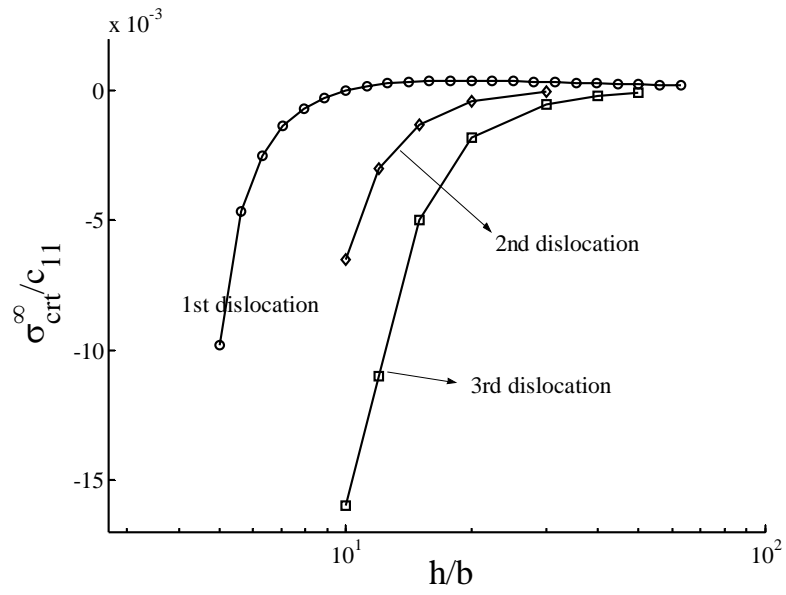


(b)

Figure 4

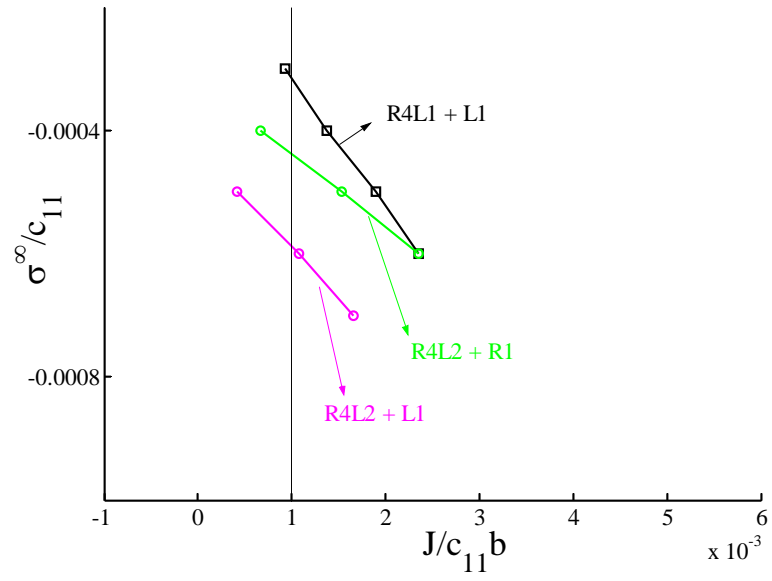


(a)

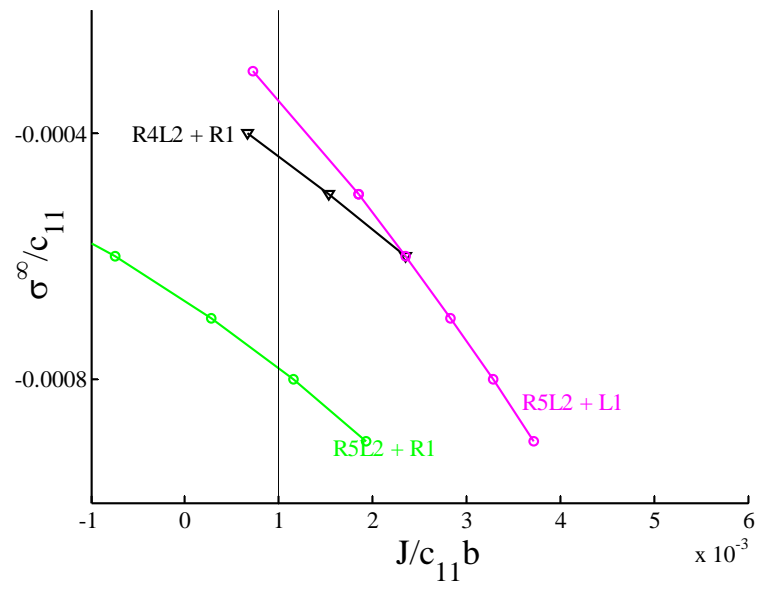


(b)

Figure 5

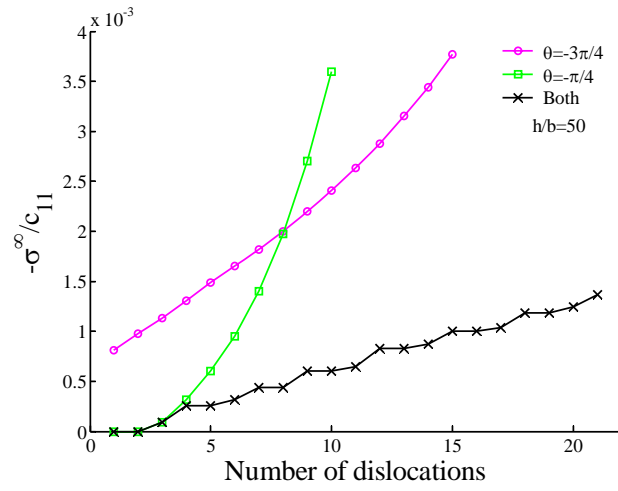


(a)

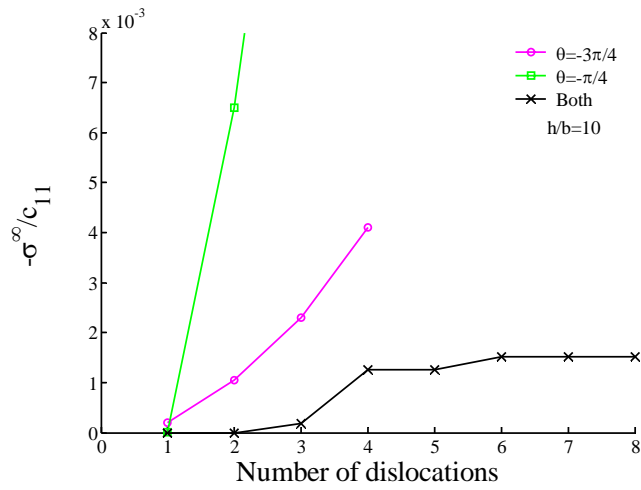


(b)

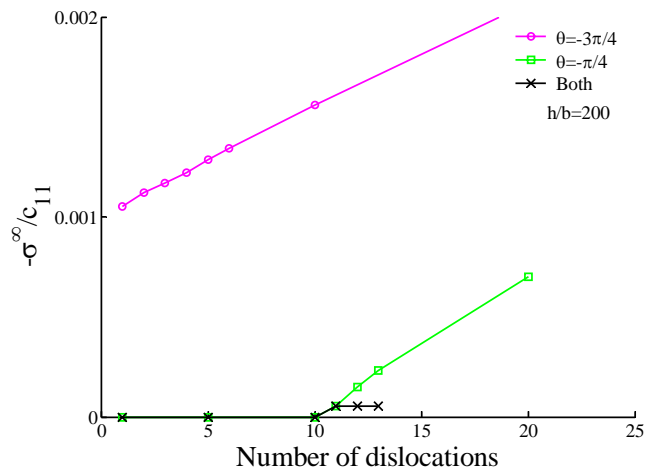
Figure 6



(a)



(b)



(c)

Figure 7

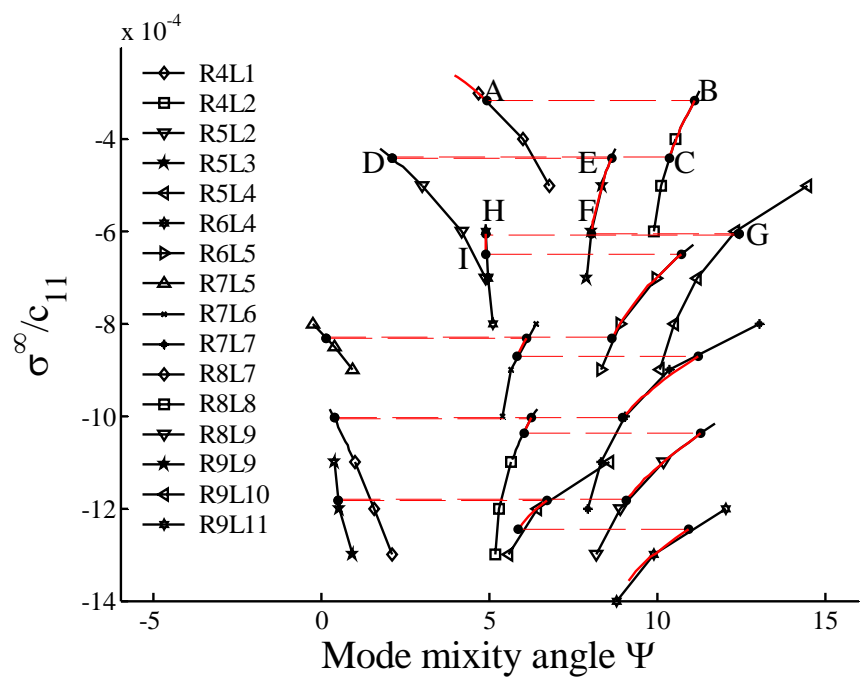
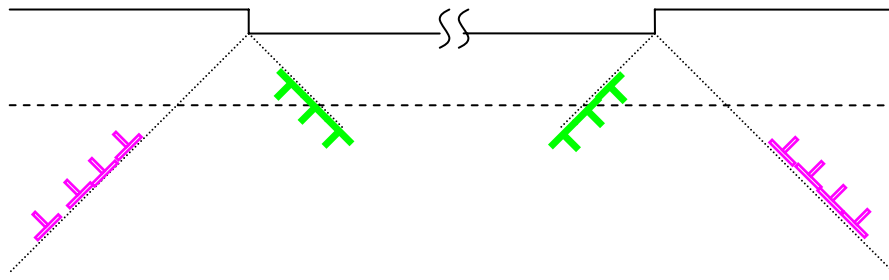
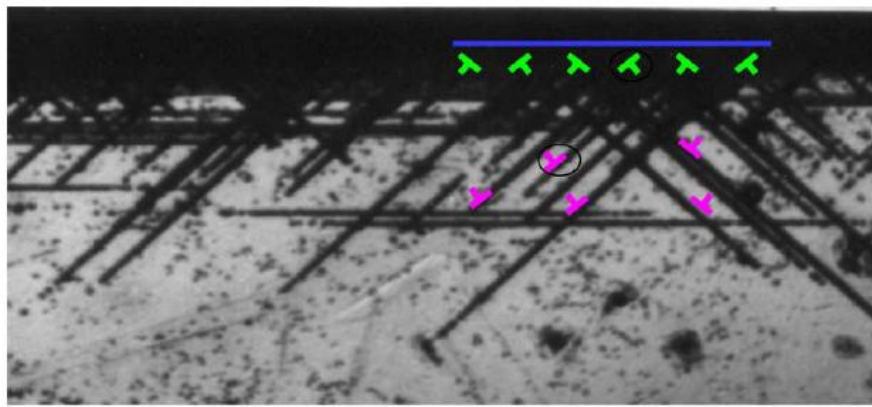


Figure 8



(a)



(b)

200  $\mu\text{m}$

Figure 9